Photoionization of Nb 3 CO and Nb 3 (CO) 2 : Is CO Molecularly or Dissociatively Adsorbed on Niobium?

ARTICLE *in* THE JOURNAL OF PHYSICAL CHEMISTRY A · FEBRUARY 2004

Impact Factor: 2.69 · DOI: 10.1021/jp036041+

7 AUTHORS, INCLUDING:

Benoit Simard
National Research Council Canada
244 PUBLICATIONS **4,343** CITATIONS
SEE PROFILE

Matthew A Addicoat
Jacobs University
38 PUBLICATIONS **300** CITATIONS
SEE PROFILE

Gregory F Metha
University of Adelaide
81 PUBLICATIONS **822** CITATIONS
SEE PROFILE

André Fielicke
Technische Universität Berlin
101 PUBLICATIONS **2,388** CITATIONS
SEE PROFILE

Photoionization of Nb_3CO and $Nb_3(CO)_2$: Is CO Molecularly or Dissociatively Adsorbed on Niobium?

David B. Pedersen,* David M. Rayner, and Benoit Simard

Steacie Institute for Molecular Sciences, National Research Council of Canada, Ottawa, Ontario K1A 0R6, Canada

Magdalene A. Addicoat, Mark A. Buntine, and Gregory F. Metha*

Department of Chemistry, University of Adelaide, Australia 5005

André Fielicke

FOM Institute for Plasma Physics, Rijnhuizen, Edisonbaan 14, 3439 MN Nieuwegein, The Netherlands

Received: July 14, 2003; In Final Form: November 25, 2003

The photoionization efficiency spectra of gas-phase Nb_3CO and $Nb_3(CO)_2$ have been acquired using a laser-ablation, photoionization mass spectrometer. The adiabatic ionization energies of the species are 5.82 ± 0.02 and 5.85 ± 0.02 eV, respectively, where error bars reflect precision, the values are accurate to within 0.1 eV. From these data and literature values of cation bond strengths, the bond energies of Nb_3-CO and Nb_3CO-CO are found to lie within the 2.8−3.4 and 1.7−1.8 eV ranges, respectively. The former is most consistent with dissociatively adsorbed CO, while the latter may correspond to molecularly or dissociatively adsorbed CO. These conclusions are supported by density-functional theory calculations. In addition to properties of Nb_3CO, the properties of the transition state to dissociative adsorption of CO have been calculated. It is found that the transition state lies lower in energy than the separated reagents. Spontaneous dissociation is expected to follow molecular adsorption of CO on Nb_3, accordingly. Over the 1540−2220 cm^{-1} range, no infrared multiphoton dissociation of Nb_3CO or $Nb_3(CO)_2$ is observed, consistent with CO being dissociatively adsorbed for both species.

1. Introduction

Adsorption of CO as a poisoning process, a side reaction, or as part of a catalytic cycle is a ubiquitous concern in heterogeneous catalysis.[1,2] With increased usage of Nb as a performance-enhancing dopant of industrial catalysts,[3,4] the number of scientific studies of the fundamental reactivity associated with Nb-containing surfaces is on the rise and multiple review articles have been published recently.[4,5,6,7] From this work, there is evidence to support the presence of both dissociatively and molecularly adsorbed CO on Nb surfaces,[8,9] but there are no conclusions regarding the conditions under which these species are formed. Thermodynamically, dissociative adsorption is thought to be strongly favored. Bond energies of the NbO and NbC diatomics are 7.53(11) and 5.39 ± 0.15 eV, respectively.[10,11] While for Nb−CO, that is, molecular CO bound to a Nb atom, a recent theoretical study reports a binding energy of 1.11 eV.[12] This latter value is comparable to the 0.99 ± 0.05-eV value measured for Nb^+-CO.[13] Although these values suggest that dissociative adsorption of CO is energetically favored, energy barriers and other kinetic bottlenecks may impede dissociative adsorption and favor formation of the molecular adduct.

Studies of Nb clusters in the gas phase are inconclusive as to the nature of adsorbed CO. In early work by Smalley and co-workers, flow tube studies conducted near room temperature at total pressures of 50−100 Torr ($7-13 \times 10^3$ Pa) found CO to stick readily to Nb_n but could not distinguish between molecularly and dissociatively adsorbed species.[14] Subsequent experimental studies of gas-phase Nb clusters have provided no definitive evidence that CO is or is not dissociatively adsorbed.[15,16] Nb clusters are among the best-defined systems with known ionization energies and dissociation energies.[17,18] Spectroscopic data for Nb_3C_2, Nb_3N_2, and Nb_3O are also available, which is rare for transition-metal cluster-adduct systems.[19−21] Interpretation of these data indicate that Nb_3O is a planar molecule, Nb_3N_2 is a doubly bridged structure, and Nb_3C_2 is a trigonal bipyramidal complex with C atoms at the axial positions. Both of the latter two structures correspond to dissociatively adsorbed N_2 and C_2 species, respectively. These data provide valuable insight into the properties of Nb clusters, for example, ionization energies, on which species have been dissociatively adsorbed. By comparison with analogous properties of species such as Nb_3CO, it may be possible to determine whether the CO is dissociatively adsorbed.

Routine use of density-functional theory (DFT) to determine thermodynamic quantities of transition-metal clusters can be impeded by the inherent complexity of the electronic structures associated with such systems. Accordingly, the ~0.5-eV (5−10 kcal mol^{-1}) accuracy generally expected of DFT calculations is likely not generally valid for transition-metal cluster systems. To gauge the expected accuracy, the reported DFT-calculated ionization energies of some ligated Nb_n species can be compared with the measured values. For Nb_3C_2, the differences between the measured ionization energy 5.046(12) eV and those calculated using different DFT methods are 0.735, 0.118, and 0.075

* To whom all correspondence should be addressed. E-mail: david.pedersen@nrc-cnrc.gc.ca (D.B.P.); greg.metha@adelaide.edu.au (G.F.M.).

10.1021/jp036041+ CCC: $27.50
Published on Web 01/16/2004

eV.[19] For Nb_3O, the difference between experimental and calculated values is found to range from 0.382 to 0.880 eV.[21] On the basis of these data, DFT-determined ionization energies for ligated Nb cluster systems of comparable size or complexity are expected to lie within ~1 eV of the experimental value.

In this paper, gas-phase Nb_3CO and $Nb_3(CO)_2$ have been generated using a laser-ablation, molecular beam, Smalley-type source. Photoionization efficiency spectra of these species have been acquired and the ionization energies of these species determined. Coupled with literature data, these ionization energies have been used to determine the bond strengths between neutral Nb_3 and CO and $(CO)_2$. Through interpretation of the photoionization efficiency spectra, infrared depletion data, and comparison with DFT calculations, CO is found to be dissociatively adsorbed on Nb_3. For $Nb_3(CO)_2$, our results are inconclusive and addition of a second CO (i.e., $Nb_3CO + CO \rightarrow Nb_3(CO)_2$) may involve molecular or dissociative adsorption.

2. Experimental Section

The laser-ablation/photoionization mass-detection apparatus has been described previously.[22] Briefly, at the point of intersection between a Nb rod and a 1 mm diameter channel, 5 mJ pulse^{-1} of 355 nm laser (Lumonics YM200) light was focused to an ~1 mm^2 spot on the surface of the rod. The laser pulse was synchronous with a He pulse of ~20 μs duration (piezoelectric valve with ~50 psi (3×10^5 Pa) backing pressure). To form CO adducts, dilute (<0.05%) mixtures of CO in He were used as the carrier gas. The ~20 μs carrier gas pulse passed through the 1 mm channel and over the rod prior to expansion into vacuum. Species generated by the laser pulse were entrained in the He and passed through a 3 cm long, 1 mm diameter nucleation channel and subsequently underwent expansion into the 10^{-5} Torr (10^{-3} Pa) vacuum of the first chamber. The molecular beam thus generated travelled the length of the chamber and passed through a 1 cm diameter orifice into a second chamber where pressures near 10^{-6} Torr (10^{-4} Pa) were maintained with a turbo pump (Balzers TPH450). In the second chamber, species were ionized using unfocused laser light of varying wavelengths. The firing of this ionization laser was synchronized with the triggers of the ablation laser and pulsed valve such that the signal intensity of Nb_3CO was a maximum. Ionization laser fluences were measured using OPHIR/NOVA and Gentec Duo/ED-500 power meters. Species ionized by the laser were then mass analyzed using a reflectron time-of-flight mass spectrometer (R. M. Jordon) with a triple multichannel plate detector. Signals were amplified (Stanford SR445), digitized (Transiac 2008), averaged 500 times, and sent to a personal computer for analysis.

To collect photoionization efficiency spectra for Nb_3, Nb_3CO, and $Nb_3(CO)_2$, the ionization laser wavelength was scanned and plots of the mass spectral signal intensity of each species vs the laser wavelength were constructed. For each of these photoionization efficiency spectra, the ionization laser power was kept constant over the range of wavelengths examined. Even so, scatterings in the data are expected as they are characteristic of laser-ablation sources; they are due primarily to inhomogeneities in the surface of the Nb rod. Normalizing the data against the Nb_3O signal intensity was found to eliminate much of the scatter in the data associated with fluctuations in source conditions. From prior work, it is known that the Nb_3O signal intensity is constant between 44550 and 46500 cm^{-1}.[21] Over the wavenumber range examined in this work, it should therefore be a good internal standard. The signal intensity of Nb_3O is sensitive to the condition of the Nb rod, which reacts with background oxygen and can change somewhat from day to day. As a standard, Nb_3O is therefore only expected to be useful over modest time frames and does not allow comparisons of absolute signal intensities taken on different days. However, over the course of a scan, for example, it can be an effective standard. As a check, the ionization energies of bare Nb clusters were measured using the normalization method and found to agree with published results (see below).

The infrared multiphoton depletion (IRMPD) experiments were performed at the Free Electron Laser Facility at the FOM Institute for Plasma Physics Rijnhuizen in The Netherlands; the apparatus has been described elsewhere.[23,24] Briefly, metal cluster species were generated in a Smalley-type pulsed-valve, supersonic expansion source similar to that used in the laser-ablation/photoionization mass-detection apparatus. Unlike the photoionization experiments, CO was injected into a small reactor tube positioned downstream of the laser-ablation region of the source. By injecting downstream, cluster species are more likely to be rovibronically quenched and thermalized to near room temperature conditions prior to exposure to the CO. Accordingly, processes that require energy to surmount an activation energy barrier are less likely to occur than if the CO was injected upstream of the plasma, as is the case for the photoionization apparatus. Upon leaving the reactor region, species expand into vacuum and travel into the extraction region of the time-of-flight mass spectrometer where they are probed. Effectively, in these experiments, the wavelength of the free-electron laser is varied, and whenever it is resonant with an infrared-active vibration of the complex, multiphoton absorption can lead to desorption of the adsorbed molecule. An accompanying depletion in the mass spectral signal intensity of the cluster-molecule adduct is observed. The method has been used successfully to deplete $Ag_n(NH_3)_m$ and thus determine portions of the infrared spectra of these species.[24]

Geometry optimization and harmonic vibrational frequency calculations were performed using DFT (B3P86 with LANL2DZ basis set) in the Gaussian 98 suite of programs.[25] This method and basis set are the same as those used by Yang et al. to calculate structures of various niobium clusters, Nb_3O, Nb_3C_2, and Nb_3N_2.[19,20,21] All structure determinations were performed without any geometry constraint. Many initial geometries were used leading to stationary points on each potential-energy surface, which were characterized as being minima or transition states by diagonalizing the second-derivative Hessian matrix to determine the number of negative eigen values (0 for minima, 1 for transition states). To verify that the transition states identified by the computational procedure actually connect to the expected minima or products, intrinsic reaction coordinate (IRC) calculations were performed, in which the paths of steepest descent (in mass-weighted Cartesian coordinates) were followed from each transition state to the connecting minima. For the neutral and cationic species, the multiplicity was maintained as doublet or singlet, respectively. Calculations on the quartet (neutral) and triplet (cation) were found to be much higher in energy.

3. Results

In Figure 1, sections of the mass spectra showing Nb_3 and Nb_3CO are shown. As seen, via seeding of CO into the carrier gas, significant amounts of Nb_3CO are formed. $Nb_3(CO)_2$ is also produced, the quantity of which can be increased somewhat by increasing the amount of CO seeded into the He carrier gas. Because of background oxygen in the vacuum system, Nb_3O is

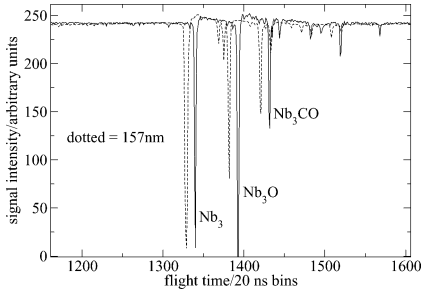

Figure 1. Sections of mass spectra showing peaks associated with Nb_3 and Nb_3CO. The two spectra were collected while ionizing with 157 and 212.5 nm, respectively. The spectra have been normalized so that the Nb_3 peak intensities are equal. With this normalization, it is easy to see that the relative amounts of Nb_3CO formed at 157 and 212.5 nm are nearly equal. The two mass spectra are offset horizontally for ease of viewing.

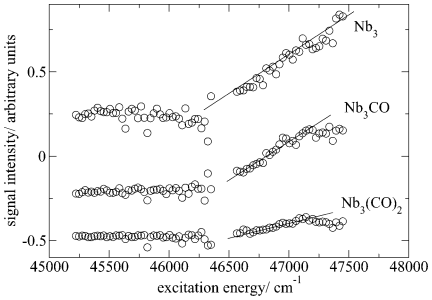

Figure 2. The photoionization efficiency spectrum of Nb_3, Nb_3CO, and $Nb_3(CO)_2$. The ionization laser power was kept to 100 ± 20 μJ pulse^{-1} at all wavelengths. Data values are shown as open circles. The solid line shows the extrapolation of the signal intensity to the baseline value. The intercept of the line with the baseline is taken to correspond to the adiabatic ionization energy. By use of this method, values of 46320 ± 150 cm^{-1} (5.74 ± 0.02 eV), 46400 ± 150 cm^{-1} (5.75 ± 0.02 eV), and 46600 ± 150 cm^{-1} (5.78 ± 0.02 eV) are found for Nb_3, Nb_3CO, and $Nb_3(CO)_2$, respectively. By correction for the temperature of the source (see text for details), the ionization energies are 5.82 ± 0.02 and 5.85 ± 0.02 eV for Nb_3CO and $Nb_3(CO)_2$, respectively. Spectra have been offset vertically for clarity.

always present. The amount present in the mass spectrum is greatly enhanced when CO is seeded into the He carrier gas. Spectra collected at both 212.5 and 157 nm are shown in Figure 1. As seen, there is no dramatic difference in the relative amounts of Nb_3CO observed at the two different wavelengths.

In Figure 2, the photoionization efficiency spectrum of Nb_3 is shown. The data points have been normalized against the Nb_3O signal intensity as described above. As seen over this wavelength region, the signal intensity falls to baseline values. The onset of signal in Figure 2 corresponds to the appearance potential, or ionization energy, of Nb_3. To precisely determine the ionization energy, the signal was linearly extrapolated to baseline values as shown. This same method is most commonly used to determine adiabatic ionization energies of metal cluster and metal cluster adduct species, thus making our results directly comparable with literature. By use of this method, a value of 46320 ± 150 cm^{-1} (5.74 ± 0.02 eV) was found. The error bar reflects the precision of the extrapolation. The absolute accuracy of the measured ionization energy is expected to lie within ~0.1 eV of the true value, as different extrapolation methods are known to yield slightly different results.[26] The 5.74 ± 0.02 eV value is slightly lower than the accepted value of 5.81 eV.[17] This result is expected, however, as ionization energies measured using room temperature ablation sources, like that used in this work, are typically ~0.1 eV lower than those measured using sources cooled with liquid nitrogen due to differences in the internal temperatures of the clusters produced in each case.[17] Accordingly, the agreement between our ionization energy and the accepted value is reasonable.

In Figure 2, the photoionization efficiency spectrum for Nb_3CO is shown. As was done for Nb_3, the ionization energy of Nb_3CO was determined by extrapolating the signal intensity to baseline values, as shown in Figure 2. By use of this method, a value of 46400 ± 150 cm^{-1} (5.75 ± 0.02 eV) was found. The photoionization efficiency spectrum for $Nb_3(CO)_2$ is also shown in Figure 2. By use of the same extrapolation method, the ionization energy of this species was found to be 46600 ± 150 cm^{-1} (5.78 ± 0.02 eV). Temperature-corrected ionization energies (see below) are 5.82 ± 0.02 and 5.85 ± 0.02 eV for Nb_3CO and $Nb_3(CO)_2$, respectively.

4. Discussion

The following discussion presents an initial examination of the experimental results and a subsequent comparison between these and DFT predictions. Through interpretation of the relative intensities of mass spectral features, the Nb_3-CO bond energies determined, the differences in shapes of the photoionization efficiency curves, and the results of the infrared depletion experiments, the nature of the adsorbed CO is determined. The conclusions reached via interpretation of the experimental results are supported by DFT calculations which have been used to predict the heights of energy barriers to dissociative adsorption of CO on the Nb_3 cluster.

4.1. Analysis of the Photoionization Data. In Figure 1, sections of mass spectra collected with ionization laser wavelengths of 157 and 212.5 nm are shown. The spectra have been normalized to the signal intensity of Nb_3 so that the relative amounts of Nb_3CO formed at the two wavelengths can be determined. As seen, the amount of Nb_3CO, relative to the amounts of Nb_3, is comparable at both wavelengths. To the extent that the relative magnitudes of the photionization cross sections of Nb_3 and Nb_3CO are similar at both wavelengths, the comparable magnitudes of the Nb_3CO peak intensities in the two spectra indicate that all of the Nb_3CO ionized at 157 nm is also ionized at 212.5 nm. That is, there are no Nb_3CO molecules present with ionization energies greater than ~5.8 eV (212.5 nm). The alternative explanation, that the photoionization cross section of Nb_3CO, relative to that of Nb_3, is much smaller (larger) at 157 nm than at 212.5 nm but the number of ionizable Nb_3CO species at 157 nm is much greater (less) such that the signal intensities observed are nearly equivalent at the both wavelengths, is possible but seems less likely. DFT results presented below support the former interpretation, suggesting that only a single isomer, the thermodynamic minimum, will be present. Along a similar vein, the signal intensity in the photoionization efficiency spectrum of Nb_3CO, shown in Figure 2, falls to zero at wavelengths longer than 219 nm (~5.7 eV) indicating that there are no species present with ionization energies less than ~5.7 eV. In combination, these results indicate that all of the Nb_3CO species observed have ionization energies between 5.7 and 5.8 eV, suggesting that either Nb_3CO or Nb_3-C-O (dissociatively adsorbed CO) is present in the experiment, *exclusively* (assuming their ionization energies differ by more than 0.1 eV). If the energy barrier to dissociative adsorption is negligible, then formation of Nb_3CO is unlikely, as spontaneous dissociation follows molecular adsorption, and only Nb_3-C-O is present. For the analogous reaction, $Nb + CO_2 \rightarrow ONbCO$, insertion of Nb into the CO bond is predicted to occur spontaneously.[27] That is, the transition state to the insertion lies lower in energy than the $Nb + CO_2$ reagents. By analogy, it is

likely that dissociative adsorption of CO also occurs spontaneously on Nb_3, in which case Nb_3-C-O is the only species present in the experiment.

To further probe the nature of the CO adsorbed on Nb_3, the ionization energy of the molecule was determined. Adducts of atoms or molecules adsorbed to metal clusters are expected to have electronic structures with features characteristic of the adsorbate. Typically, a measure of the ionization energy reflects this characteristic electronic structure and provides some insight into the nature of the species adsorbed to the metal cluster surface. For Nb_3CO, the ionization energy is found to be 5.75 $\pm$ 0.02 eV via an extrapolation of the photoionization efficiency spectrum shown in Figure 2, as discussed above. To account for the relatively high internal energy of the species generated in the laser-ablation source, however, a correction factor needs to applied to this value. By use of Nb_3 as a calibration standard (see above), the ionization energies extrapolated from the photoionization efficiency spectra are 0.07 eV too low. This value reflects the amount of internal energy in the clusters generated by the room-temperature source. To facilitate comparison with literature values, we correct for this internal energy by adding 0.07 eV to the ionization energies extrapolated from the photoionization efficiency spectra. Accordingly, the temperature-corrected ionization energy of Nb_3CO is 5.82 $\pm$ 0.02 eV.

With the addition of the Nb_3CO photoionization data to the data available, a near-complete picture of the thermodynamics associated with adsorption of CO to Nb_3 can be drawn and the bond energy of Nb_3-CO determined. The relevant data are (1) the binding energy of CO to Nb_3^+,[28] (2) the ionization energy of Nb_3,[17] and (3) our measured ionization energy of Nb_3CO. From these data, the bond energy of Nb_3-CO can be calculated if the assumption is made that the ionization energies extrapolated from the photoionization efficiency spectra are good approximations of the adiabatic ionization energies.

$$\begin{array}{ccc} Nb_3CO^+ - DE_{Nb_3CO^+} \rightarrow Nb_3^+ + CO \\ \uparrow IP_{Nb_3CO} \qquad\qquad \downarrow -IP_{Nb_3} \\ Nb_3CO \leftarrow BE_{Nb_3CO} - Nb_3 + CO \end{array} \qquad (1)$$

In eq 1, the relevant thermodynamic cycle is shown from which it follows that

$$IP_{Nb_3} - IP_{Nb_3CO} = -BE_{Nb_3CO} - DE_{Nb_3CO^+} \qquad (2)$$

where $DE_{Nb_3CO^+}$ and $-BE_{Nb_3CO}$ are the energies required to remove CO from Nb_3CO^+ and to add CO to Nb_3, respectively. IP_{Nb_3CO} is the ionization energy of Nb_3CO and IP_{Nb_3} is the ionization energy of Nb_3. Substitution of the known values (IP_{Nb_3CO} = 5.82 $\pm$ 0.02 eV, IP_{Nb_3} = 5.81 eV, and 2.8 eV < $DE_{Nb_3CO^+}$ < 3.4 eV) into eq 2 yields a value of 2.8−3.4 eV for BE_{Nb_3CO}. Noting that Zheng and Yang[28] also employed a room-temperature ablation source to determine the Nb_3^+-CO bond strength, it is appropriate to apply the 0.07-eV correction factor such that the temperature-corrected bond energy for Nb_3CO is 2.9−3.5 eV. Literature values of the bond energy of molecular CO bound to Nb_4, as predicted by DFT, lie in the 1.17−2.87 eV range.[29] There is a slight overlap between this and the experimental range, suggesting that CO may be molecularly adsorbed on Nb_3. It is more plausible, however, that the CO is dissociatively adsorbed on Nb_3.

A similar analysis can be performed for $Nb_3(CO)_2$, yielding a bond energy of 1.7−1.8 eV. For this species, the measured Nb_3CO^+-CO bond energy is 1.82−1.94 eV,[28] significantly lower than the 2.9−3.5 eV value measured for the Nb_3^+-CO. The large difference in bond energy indicates that the nature of the bond formed with the second CO is significantly different than that formed with the first. The difference is explored with DFT below.

Although the spectra shown in Figure 2 are void of vibronic structure, preventing assignment of spectral features to specific vibrational modes, the overall shapes of the photoionization efficiency spectra do yield some insight into the geometry of the neutral as compared with that of the cation. Via comparison with DFT predictions, made below, this information can be used to determine the nature of the adsorbed CO. Near threshold, the signal intensity observed corresponds to the ground-state neutral to ground-state cation optical transition. To first order, changes in the photoionization cross section of this transition are attributable to changes in the Franck−Condon factors associated with each of the vibrational modes contributing to the spectrum. Thus, the shape of the spectrum reflects the Franck−Condon overlap between the two electronic states. In a cold beam where all clusters are in their ground vibrational states, a sharp increase in the signal intensity at threshold is indicative of good Franck−Condon overlap between this ground vibronic state and the ground vibronic state of the cation. In this case, optical transitions between the neutral ground state and higher vibrational levels of the ground electronic state of the cation have much lower probability due to poor Franck−Condon overlap, and scanning the laser to higher energy manifests no significant change in the observed signal intensity. Accordingly, the sharp step in the photoionization efficiency spectrum is followed by a plateau where changes in wavelength manifest no increase in signal intensity. At even higher laser energies, the signal intensity may rise even higher than the plateau level as ions produced via transitions to electronically excited states of the cation begin to contribute to the observed signal, and in some cases, these types of transitions may mask the plateau effect. However, we are only concerned here with transitions involving the ground electronic states of Nb_3CO, $Nb_3(CO)_2$, and their respective cations, the spectra of which both have near-threshold plateaus. In these cases, the narrow span between the onset of signal and the onset of the plateau reflects the goodness of the Franck−Condon overlap between the two ground states; a narrow span indicates that transitions to only one or two vibrational states contribute to the observed ion signal and the overlap is good.

In Figure 2, the threshold regions of the photoionization efficiency spectra of Nb_3CO and $Nb_3(CO)_2$ are shown and the spans between onset of signal and onset of plateau for both species are seen to be relatively narrow, 900 cm^{-1}. To put this value in perspective, we compare it with the spectra of other complexes of Nb_3. Nb_3C_2, for example, has a relatively long gap between the onset of signal and the onset of plateau in the photoionization efficiency spectrum, spanning 1200 cm^{-1}. This long gap has been attributed to a long, thermally broadened, progression. Large differences in the geometries of the ground electronic states of the neutral and cation are thought to manifest the long progression. For Nb_3O, on the other hand, the geometries of the neutral and cation are very similar, the Franck−Condon overlap is good, and the gap between the onset of signal and the onset of plateau is only 500 cm^{-1}.[21] By analogy, the relatively narrow gaps for Nb_3CO and $Nb_3(CO)_2$ in Figure 2 suggest that the ground electronic states of the neutrals and cations of these species have similar geometries. Accordingly, interpretation of the shapes of the photoionization efficiency spectra of Nb_3CO and $Nb_3(CO)_2$ indicates that, whatever the nature of the CO, there is little difference in the geometries of the ground electronic states of the neutral and

cation forms of these species. DFT calculations discussed below find these results most consistent with the CO being dissociatively adsorbed in Nb_3CO.

The relatively narrow span between the onset of signal and the onset of the plateau near the ionization threshold, as reflected in the photoionization efficiency spectrum, indicates good Franck−Condon overlap between the ground states of the Nb_3CO neutral and cation. Accordingly, the geometries of the two charge states of Nb_3CO are very similar. The small difference between the ionization energy of Nb_3CO and Nb_3 indicates that the Nb_3CO and Nb_3CO^+ bond strengths are nearly equal, as seen in eq 1. To the extent that the charge of the cation is localized on the Nb_3 moiety, as expected, the similar bond strengths and geometries of Nb_3CO and Nb_3^+CO indicate that charge on the Nb_3 cluster has little effect on the nature of the Nb−CO bonds. By use of analogous arguments, the same is true for (Nb_3CO)−CO and (Nb_3^+CO)−CO. That is, the nature of the CO−(Nb_3CO) bond is not affected by the charge on the Nb_3 moiety. Similarly, from the literature, the bond strengths of Nb−CO and Nb^+−CO are nearly equal.[12,13] In this context, the interactions of CO with Nb particles may be expected to be relatively insensitive to charge-altering effects such as electron withdrawal from the particle by an electrophilic supporting medium. However, systems with potential for forming Nb_n−C and Nb_nO−C bonds are found to be sensitive to the support. For example, the interactions of alkanes with niobia particles supported on silica, alumina, titania, and zirconia are found to be sensitive to the nature of the support.[31,32] The discrepancy between the gas-phase and solid-phase results may arise from the difference in oxidation states of the metal, which are relatively small for the Nb_n−CO species but near +5 for the niobia used as the supported catalyst.

The presence of molecularly adsorbed CO on Nb_n and Nb_n^+ was also probed by using infrared multiphoton depletion (IRMPD) spectroscopy. Over the 1540−2220 cm^{-1} range, no depletion of the mass spectral peaks associated with Nb_3CO or $Nb_3(CO)_2$ was observed. The most plausible reason for the absence of depletion is that the CO is dissociatively adsorbed in both cases. In these experiments, CO was injected into a reactor tube downstream from the ablation source under near-room-temperature conditions. Thus, any dissociative adsorption of CO that occurs does so outside of the high-energy conditions of the ablation area, in which case either the barrier to dissociative adsorption is small or lies lower in energy than the separated reagents. This result is consistent with the barrierless reaction path predicted for the analogous insertion reaction $Nb + CO_2 \rightarrow ONbCO$.[27]

The experimental results can be summarized as follows. From analysis of the mass spectra, it is clear that a single form of Nb_3−CO, either dissociatively or molecularly adsorbed, is present in the experiment. If the transition state to dissociative adsorption lies lower in energy than the separated $Nb_3 + CO$ reagents, as comparison with the analogous insertion reaction $Nb + CO_2 \rightarrow ONbCO$ suggests,[27] then the dissociatively adsorbed Nb_3−C−O form is present. Ionization of this species manifests no large changes in geometry, in accord with the relatively narrow spans between onset of signal and onset of plateau in the photoionization efficiency spectrum near the ionization threshold. A similar result is obtained for $Nb_3(CO)_2$. The experimentally determined, temperature-corrected Nb_3−CO bond energy is found to be 2.9−3.5 eV. Comparison with the theoretical values of 1.17−2.87 eV, for CO molecularly adsorbed to Nb_4, is inconclusive. The results of the IRMPD experiments, where no depletion of Nb_3CO or $Nb_3(CO)_2$ is observed over the 1540−2220 cm^{-1} range, are most consistent with the CO being dissociatively adsorbed for both species.

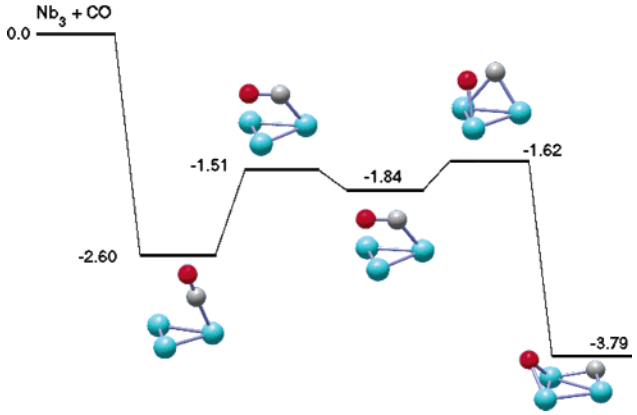

Figure 3. A partial potential-energy profile for CO adsorption on Nb_3 as predicted by DFT (see text for details). The left asymptote corresponds to separated Nb_3 and CO. The energies of dissociatively and molecularly adsorbed CO are shown as are the energies of the transition states to molecular and dissociative adsorption. Geometries of the molecularly and dissociatively adsorbed species are given. The corresponding bond lengths are in Table 1. The geometries of the transition states are also shown. Energies are given in eV units.

TABLE 1: Geometric Parameters of Nb_3, Nb_3^+, Nb_3CO, and Nb_3CO^+ as Predicted by DFT[a]

species	bond	neutral length/Å	cation length/Å
Nb_3	Nb−Nb′	2.390	2.485
	Nb−Nb″	2.457	2.274
	Nb′−Nb″	2.291	2.483
Nb_3CO	C−O	1.229	1.223
	C−Nb	2.518	2.215
	C−Nb′	1.990	2.216
	Nb−Nb′	2.496	2.434
	Nb−Nb″	2.325	2.434
	Nb′−Nb″	2.454	2.434
Nb_3−C−O	C−Nb′	1.974	1.952
	C−Nb″	1.974	1.952
	O−Nb′	2.006	1.996
	O−Nb″	2.005	1.996
	Nb−Nb′	2.402	2.415
	Nb−Nb″	2.400	2.415
	Nb′−Nb″	2.881	2.832

[a] See text for details.

4.2. DFT Results. The most stable confomers (global minima) of Nb_3CO and Nb_3−C−O, molecularly and dissociatively adsorbed CO, respectively, determined using DFT are shown in Figure 3 with bond lengths shown in Table 1. In addition to these, the geometric structure of Nb_3 was predicted and its ionization energy determined as a calibration. The adiabatic ionization energy predicted for Nb_3 is 6.8 eV in agreement, within the approximately 1 eV error expected (see above), with the accepted value of 5.81 eV.[17] Goodwin and Salahub also found *state-of-the-art* DFT to overestimate the ionization energies of Nb clusters, predicting an ionization energy of ~6.3 eV for Nb_3.[30] For Nb_3CO, the predicted adiabatic ionization energies are 6.6 and 6.8 eV for molecularly and dissociatively adsorbed CO, respectively. Both values exceed the experimental value and agree with the measured value of 5.82 ± 0.02 eV, within the ~1 eV error expected (see above). As both values agree with experiment, direct comparison of the DFT and experimental ionization energies cannot be used to distinguish molecular from dissociatively adsorbed analogues of Nb_3CO.

Comparison of the DFT-predicted geometries with the conclusions reached from interpretation of the shapes of the

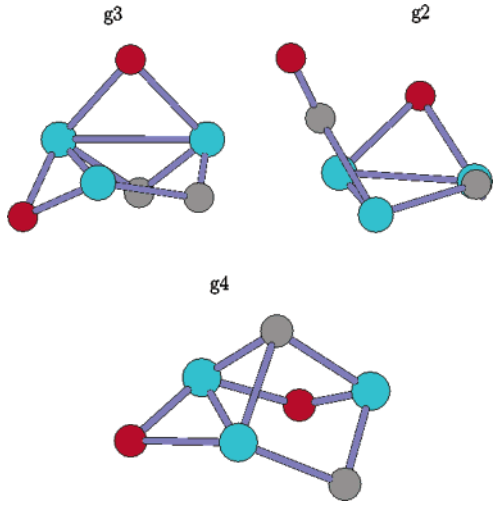

Figure 4. Geometric structures of $Nb_3-C-O-CO$ as predicted by DFT. Bond lengths are given in Table 2.

photoionization efficiency curves indicates that CO is dissociatively adsorbed on Nb_3. From Table 1 it is seen that DFT predicts little change in geometry upon ionization of Nb_3-C-O but a significant change upon ionization of Nb_3CO (molecularly adsorbed CO). The large change in geometry predicted for Nb_3CO is inconsistent with the relatively narrow progression (small gap between onset of signal and onset of plateau) in the photoionization efficiency spectrum of Nb_3CO, shown in Figure 2. The DFT results, suggest, therefore, that the photoionization efficiency spectrum is not that of Nb_3CO. The spectrum is more likely that of Nb_3-C-O, for which a much smaller change in geometry is predicted to accompany ionization.

The DFT-predicted formation energies of species relevant to the reaction of CO with Nb_3 are seen in Figure 3. Both molecular and dissociated forms of adsorbed CO are predicted to lie lower in energy than the separated reagents with the dissociated confomer being the thermodynamic minimum. The transition state to formation of this species is predicted to lie lower in energy than the separated Nb_3 + CO reagents. In the low-pressure limit or at elevated temperatures, dissociation will occur spontaneously. The prediction that dissociation occurs spontaneously is analogous to the conclusions reached for Nb + CO_2.[27] Under the energetic conditions of the laser-ablation source, quenching of the entire population of nascent Nb_3CO is improbable and, in the context of the potential energy surface shown in Figure 3, at least some conversion to Nb_3-C-O is expected to occur. As only a single species is present in the experiment, as determined above, it must be the case that the entire population is converted and it is Nb_3-C-O that is observed, exclusively. In this context, the agreement between theory and experiment is compelling evidence that CO spontaneously dissociates upon adsorption of Nb_3.

Similar results are found for $Nb_3(CO)_2$. Addition of CO to Nb_3-C-O is found to be exothermic for both molecularly and dissociatively adsorbed forms. The predicted geometries of these species are shown in Figure 4 and Table 2. The formation energies of the species, relative to Nb_3-C-O, are −2.1, −3.2, and −4.1 eV for *g*2, *g*3, and *g*4, respectively. As is the case for Nb_3CO, the ionization energies predicted for both molecular and dissociated forms exceed the experimental value. However, both molecularly and dissociatively adsorbed species, *g*2 and *g*4, are predicted to have ionization energies of ∼6.8 eV, equal to the value predicted for Nb_3-C-O. This result is compatible with experiment where the Nb_3CO and $Nb_3(CO)_2$ are found to have very similar ionization energies. *g*3 is predicted to have an ionization of 5.9 eV, significantly different than that of Nb_3-C-O. For both *g*2 and *g*4, there is little change in geometry predicted to accompany ionization (data not shown), consistent with the overall shape of the photoionization efficiency spectrum as discussed above. Overall, the DFT results for both molecular and dissociatively adsorbed forms are compatible with the experimental results and no conclusions can be drawn regarding the nature of the CO adsorbed to Nb_3-C-O.

TABLE 2: Geometric Parameters of $Nb_3-C-O(CO)$ as Predicted by DFT[a]

bond	length in *g*2/Å	length in *g*3/Å	length in *g*4/Å
Nb−Nb′	2.530	2.753	2.498
Nb−Nb″	2.471	2.699	2.863
Nb′−Nb″	2.842	3.028	2.846
Nb−C		1.907	2.059
Nb″−C	1.956	1.943	2.045
Nb′−C	1.991		2.082
Nb′−C′		1.909	1.979
Nb″−C′		1.954	1.896
Nb−O	2.049	1.997	1.946
Nb′−O		1.958	2.061
Nb−O′		1.983	1.953
Nb″−O′		1.997	1.978
Nb″−O	1.907		
Nb′−C_m	2.028		
C_m-O_m	1.217	2.483	

[a] See text for details.

5. Summary and Conclusions

The results of photoionization and multiphoton infrared depletion studies strongly suggest that CO is dissociatively adsorbed on Nb_3 thus forming Nb_3-C-O. In addition to these data, DFT calculations predict that the transition state to dissociative adsorption of CO on Nb_3 lies lower in energy than the separated Nb_3 + CO reagents. Rapid dissociative adsorption of CO should follow molecular adsorption, accordingly. The ionization energy of the Nb_3CO adduct is found to be 5.82 ± 0.02 eV, less than 0.01 eV higher than the ionization energy of Nb_3.[17] On the basis of thermodynamic cycles, the small difference is evidence that there is little change in the Nb_3-C and Nb_3-O bond strengths upon ionization, suggesting that charge has relatively little effect on the nature of these bonds. The bond strength of neutral Nb_3CO is found to be 2.8−3.4 eV. In this context, the Nb_3CO system constitutes an example of the noneffect of charge on cluster−reagent bonding. A similar result has been obtained for $Nb_3(CO)_2$, the ionization energy of which is 5.85 ± 0.02 eV. This value is comparable to that of Nb_3CO. Based on thermodynamic cycles, the (Nb_3CO)-CO bond strength also does not change significantly upon ionization. The neutral is found to have a value of 1.8 to 1.9 eV, significantly different than the bond strength of Nb_3-CO. DFT results suggest that both molecularly and dissociatively adsorbed analogues of $Nb_3(CO)_2$ are compatible with the experimental results. Unlike Nb_3CO, where all of our results indicate that the CO is dissociated, for $Nb_3(CO)_2$ the DFT results are inconclusive. The IRMPD results, however, suggest that both CO molecules are dissociatively adsorbed.

References and Notes

(1) Henrici-Olive, G.; Olive, S. *The Chemistry of the Catalyzed Hydorgenation of Carbon Monoxide*; Springer-Verlag: Berlin, 1984.

(2) *New Trends in CO Activation*; Guczi, C., Ed.; Elesevier: Amsterdam, 1991.

(3) Ushikubo, T. *Catal. Today* **2000**, *57*, 3.
(4) Tanabe, K. *Catal. Today* **1993**, *16*, 333.
(5) Nowak, I.; Ziolek, M. *Chem. Rev.* **1999**, *99*, 3603.
(6) Tanabe, K.; Okazaki, S. *Appl. Catal. A* **1995**, *133*, 191.
(7) Tanabe, K. *Catal. Today* **1990**, *8*, 1.
(8) Cabrera, A. L.; Garrid-Molina, W.; Colino, J.; Lederman, D.; Schuller, I. K. *Phys. Rev. B* **1997**, *55*, 13999.
(9) Park, H. G.; Abbaschian, R. *Metall. Mater. Trans. B* **1997**, *28*, 455.
(10) Loock, H. P.; Simard, B.; Wallin, S.; Linton, C. *J. Chem. Phys.* **1998**, *109*, 8980.
(11) Simard, B.; Presunka, P. I.; Loock, H. P.; Berces, A.; Launila, O. *J. Chem. Phys.* **1997**, *107*, 307.
(12) Tan, H.; Liao, M.; Dai, D.; Balasubramanian, K. *Chem. Phys. Lett.* **1998**, *297*, 173.
(13) Sievers, M. R.; Armentrout, P. B. *Int. J. Mass Spectrom. Ion Proc.* **1998**, *179/180*, 103.
(14) Morse, M. D.; Geusic, M. E.; Heath, J. R.; Smalley, R. E. *J. Chem. Phys.* **1985**, *83*, 2293.
(15) Holmgren, L.; Andersson, M.; Rosen, A. *Surf. Sci.* **1995**, *331*, 231.
(16) Mwakapumba, J.; Ervin, K. M. *Int. J. Mass. Spectrom. Ion Proc.* **1997**, *161*, 161.
(17) Knickelbein, M. B.; Yang, S. *J. Chem. Phys.* **1990**, *93*, 5760.
(18) Loh, S. K.; Lian, L.; Armentrout, P. B. *J. Am. Chem. Soc.* **1989**, *111*, 3167.
(19) Yang, D. S.; Zgierski, M. Z.; Berces, A.; Hackett, P. A.; Roy, P.-N.; Martinez, A.; Carrington, T., Jr.; Salahub, D. R.; Fournier, R.; Pang, T.; Chen, C. *J. Chem. Phys.* **1996**, *105*, 10663.
(20) Yang, D. S.; Zgierski, M. Z.; Berces, A.; Hackett, P. A.; Martinez, A.; Salahub, D. R. *Chem. Phys. Lett.* **1997**, *227*, 71.
(21) Yang, D. S.; Zgierski, M. Z.; Rayner, D. M.; Hackett, P. A.; Martinez, A.; Salahub, D. R.; Roy, P. N.; Carrington, T., Jr. *J. Chem. Phys.* **1995**, *103*, 5335.
(22) Jakubek, Z. J.; Simard, B. *J. Chem. Phys.* **2000**, *112*, 1733.
(23) von Helden, G.; Kirilyuk, A.; van Heijnsbergen, D.; Saratokov, B.; Duncan, M. A.; Meijer, G. *Chem. Phys.* **2000**, *31*, 31.
(24) Simard, B.; Denommee, S.; Rayner, D. M.; van Heijnsbergen, D.; Meijer, G.; von Helden, G. *Chem. Phys. Lett.* **2002**, *357*, 195.
(25) Frisch, M. J.; Trucks, G. W.; Schlegel, H. B.; Scuseria, G. E.; Robb, M. A.; Cheeseman, J. R.; Zakrzewski, V. G.; Montgomery, J. A., Jr.; Stratmann, R. E.; Burant, J. C.; Dapprich, S.; Millam, J. M.; Daniels, A. D.; Kudin, K. N.; Strain, M. C.; Farkas, O.; Tomasi, J.; Barone, V.; Cossi, M.; Cammi, R.; Mennucci, B.; Pomelli, C.; Adamo, C.; Clifford, S.; Ochterski, J.; Petersson, G. A.; Ayala, P. Y.; Cui, Q.; Morokuma, K.; Malick, D. K.; Rabuck, A. D.; Raghavachari, K.; Foresman, J. B.; Cioslowski, J.; Ortiz, J. V.; Stefanov, B. B.; Liu, G.; Liashenko, A.; Piskorz, P.; Komaromi, I.; Gomperts, R.; Martin, R. L.; Fox, D. J.; Keith, T.; Al-Laham, M. A.; Peng, C. Y.; Nanayakkara, A.; Gonzalez, C.; Challacombe, M.; Gill, P. M. W.; Johnson, B. G.; Chen, W.; Wong, M. W.; Andres, J. L.; Head-Gordon, M.; Replogle, E. S.; Pople, J. A. *Gaussian 98*; Gaussian, Inc.: Pittsburgh, PA, 1998.
(26) Akola, J.; Hakkinen, H.; Manninen, M. *Eur. Phys. J. D* **1999**, *9*, 179.
(27) Chen, M.; Wang, X.; Zhang, L.; Qin, Q. *J. Phys. Chem. A* **2000**, *104*, 7010−7015.
(28) Zheng, L.; Yang, S. *Cuihua Xuebao* **1988**, *9*, 260.
(29) Gronbeck, H.; Rosen, A.; Andreoni, W. *Z. Phys. D* **1996**, *40*, 206.
(30) Goodwin, L.; Salahub, D. R. *Phys. Rev. A* **1993**, *47* (2), R774.
(31) Deo, G.; Wachs, I. E. *J. Catal.* **1994**, *146*, 323.
(32) Wachs, I. E.; Jehng, J. M.; Deo, G.; Hu, H.; Auora, N. *Catal. Today* **1991**, *28*, 199.